Journal of Biomolecular NMR (2005) 31: 295–310
DOI 10.1007/s10858-005-1718-z
© Springer 2005

Article

Detection of dynamic water molecules in a microcrystalline sample of the SH3 domain of α-spectrin by MAS solid-state NMR

Veniamin Chevelkov[a], Katja Faelber[b,c], Anne Diehl[a], Udo Heinemann[b,c], Hartmut Oschkinat[a,c] & Bernd Reif[a,d,*]

[a]*Forschungsinstitut für Molekulare Pharmakologie (FMP), Robert-Rössle-Str. 10, 13125, Berlin, Germany;* [b]*Max-Delbrück-Centrum für Molekulare Medizin, Robert-Rössle-Str. 10, 13125, Berlin, Germany;* [c]*Institut für Chemie / Kristallographie, Freie Universität Berlin, Takustr. 6, 14195, Berlin, Germany;* [d]*Charité Universitätsmedizin, D-10115, Berlin, Germany*

Received 25 October 2004; Accepted 25 January 2005

Key words: crystalline proteins, deuteration, dynamics, MAS solid state NMR, uniform isotopic enrichment, water, X-ray crystallography

Abstract

Water molecules are a major determinant of protein stability and are important for understanding protein–protein interactions. We present two experiments which allow to measure first the effective T_2 decay rate of individual amide proton, and second the magnetization build-up rates for a selective transfer from H_2O to H^N using spin diffusion as a mixing element. The experiments are demonstrated for a uniformly ^2H, ^{15}N labeled sample of a microcrystalline SH3 domain in which exchangeable deuterons were back-substituted with protons. In order to evaluate the NMR experimental data, as X-ray structure of the protein was determined using the same crystallization protocol as for the solid-state NMR sample. The NMR experimental data are correlated with the dipolar couplings calculated from H_2O–H^N distances which were extracted from the X-ray structure of the protein. We find that the H^N T_2 decay rates and H_2O–H^N build-up rates are sensitive to distance and dynamics of the detected water molecules with respect to the protein. We show that qualitative information about localization and dynamics of internal water molecules can be obtained in the solid-state by interpretation of the spin dynamics of a reporter amide proton.

Introduction

The interaction of water with proteins is a major determinant of protein stability and is important for understanding protein–protein interactions. In protein crystal structures, many water molecules are found to be closely associated with polar surface groups and may confer correlated dynamical behaviour of these groups. Moreover, water molecules play a very important role in the functionality of many membrane proteins like water and ion channels, and proton pumps, such as bacteriorhodopsin and secondary transporters. The discovery and characterization of channels in cell membranes, for which the Nobel price for Chemistry in 2003 was awarded to Peter Agre and Roderick MacKinnon, has an on-going impact on the study of membrane proteins in general. Even though many structural aspects of water and ion channels could be clarified (Murata et al., 2000; Zhou et al., 2001), questions concerning the details of the transport mechanism remain to be answered (Saparov and Pohl, 2004). Solid-state NMR is perfectly suited to address these problems due to its sensitivity to the local environment of a given spin. Characterization of mobile water in MAS solid-state NMR was pioneered by Griffin and

*To whom correspondence should be addressed. E-mail: reif@fmp-berlin.de

co-workers, who detected water molecules in the vicinity of the Schiff-base nitrogen in bacteriorhodopsin (Harbison et al., 1988). High resolution MAS solid-state NMR developed rapidly over the last few years and allows for assignment (McDermott et al., 2000; Pauli et al., 2000, 2001) and structure determination of small peptides and proteins (Castellani et al., 2002; Rienstra et al., 2002). We and others have shown that deuteration of proteins is a useful approach to yield high sensitivity in proton detected experiments (Chevelkov et al., 2003; Paulson et al., 2003b; Reif and Griffin, 2003), and allows the determination of long range $^{1}H^{N}$, $^{1}H^{N}$ distances between back exchanged amide protons (Reif et al., 2001; Paulson et al., 2003a; Reif et al., 2003). In this article, we suggest the use of deuteration to study distance and dynamics of water molecules in detail. Deuteration is required in order to suppress strong intramolecular proton–proton dipolar interactions which would perturb weaker interactions between the protein and the water molecules of interest.

It was demonstrated in solution state NMR that information about hydration dynamics can be obtained from nuclear Overhauser effects (NOEs) between water and protein protons (Otting and Wüthrich, 1989; Clore et al., 1990; Otting, 1997). Tightly bound water molecules can be site-specifically localized. If their correlation time is long enough ($\omega\tau_c > 1.13$), they give rise to a negative NOE which has the same sign as the diagonal peak. A differentiation is achieved by a comparison of ROESY and NOESY type experiments. Complementary information on the dynamics of internal water molecules can be obtained from magnetic relaxation dispersion measurements (Noack, 1986; Noack et al., 1997). This method makes use of a differential rotational correlation time of water molecules which gives rise to a characteristic frequency dependence of the longitudinal relaxation rate R_1 especially of quadrupolar nuclei like ^{2}H and ^{17}O, and allows the determination of the lifetime of water molecules bound in the interior of a protein. This lifetime is strongly temperature-dependent and was estimated to be in the order of microseconds at room temperature (Denisov et al., 1996; Gottschalk et al., 2001; Halle and Denisov, 2001). Buried water molecules exchange with external bulk water as a result of protein conformational fluctuations. Motion in this time regime ($\tau_c \approx 1\mu s$) should therefore induce relaxation in neighbouring H^{N} resonances due to fluctuations of dipole–dipole interactions.

We present here a qualitative description of the water dynamics in a protein in the solid-state. The dynamics are indirectly monitored by the efficiency of magnetization transfer between a water molecule and a reporter amide proton, and by the T_2 relaxation of the amide protons. Conclusions are drawn by interpretation of the solid-state NMR data in view of an experimental X-ray structure. The obtained resolution of 1.49 Å allows the refinement of water molecules in the structure. The current study was motivated by the observation that certain cross peaks were missing when proton–proton homonuclear dipolar decoupling was omitted during evolution of proton chemical shifts in a ^{1}H, ^{15}N correlation experiment (Chevelkov et al., 2003). Recently, Lesage and Böckmann have reported correlations between side chain carbon resonances and water protons (Lesage and Böckmann, 2003). These correlations were predominantly observed for Tyr, Thr, Ser, Lys and His residues with labile hydroxyl, imidazole ring, or side-chain amine protons, and were attributed to chemical exchange between these labile protons and water. Correlations between amide protons and water were observed previously by Zilm and co-workers (Paulson et al., 2003a). However, no attempt was made to study these water molecules in detail. The experiments presented here are sensitive to distance and dynamics of the detected water molecules with respect to the protein. We show here for the first time that qualitative information about localization and dynamics of internal water molecules can be obtained in the solid-state by interpretation of the spin dynamics of a reporter amide proton.

Materials and methods

Sample preparation

The SH3 protein was overexpressed and purified as described by Castellani et al., 2002. Crystals for X-ray structure determination were grown to a size of $100 \times 150 \times 2000\ \mu m^3$ with the hanging drop vapour diffusion method using 100 mM ammonium sulphate titrated to a pH value of 7.2. For solid-state NMR experiments, crystals grew in a

large scale sitting drop (500 μl) under the same conditions.

Solid-state NMR spectroscopy

^{1}H T_2 filter dephasing experiments were performed on a 600 MHz Bruker-Avance wide-bore spectrometer equipped with a 4 mm triple resonance probe. H_2O–H^N spin diffusion experiments were recorded on a 400 MHz Bruker-Avance wide-bore spectrometer equipped with a 4 mm triple resonance probe. All experiments were carried out at 280 K. Approximately 9 mg of protein was filled into a 4 mm NMR rotor. The MAS frequency was set to 10 kHz. Both experiments are based on a ^{1}H, ^{15}N correlation experiment to resolve all amide sites in the protein backbone (Figure 1). During the proton evolution period in the indirect dimension, ^{1}H, ^{1}H homonuclear decoupling was achieved by application of PMLG-9 (Vinogradov et al., 1999) using a proton radio frequency field of 81 kHz and a t_1^{max} of 15 ms. The ^{1}H, ^{15}N scalar coupling, as well as possible residual heteronuclear dipolar broadening, was removed by implementation of a ^{15}N 180° pulse in the middle of t_1 (Lesage and Emsley, 2001). After the indirect evolution period, polarization is transferred via CP from ^{1}H to ^{15}N. The CP mixing time was set to 160 μs in order to restrict magnetization transfer between directly bonded nuclei. During detection, TPPM (Bennett et al., 1995) was applied on the ^{1}H channel for heteronuclear decoupling using a rf field strength of 90 kHz. In the T_2 filter experiment, a rotor synchronized 180° pulse is implemented in the center of the filtering period to refocus all inhomogeneous interactions. In the H_2O–H^N spin diffusion experiment, a REDOR filtering element of six rotor periods duration is implemented to dephase magnetization of nitrogen-bonded protons. At the same time, PMLG is applied to protons to suppress dipole–dipole interactions of the proton network. The optimum duration of the REDOR dephasing period was numerically optimized using SIMPSON (Bak et al., 2000). The assignments of the ^{1}H, ^{15}N

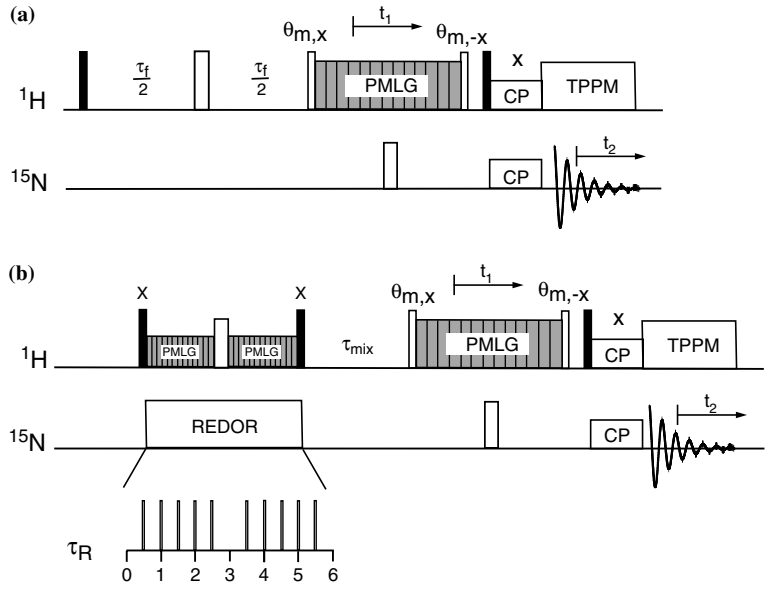

Figure 1. NMR pulse sequences for localization of water molecules bound to proteins by MAS solid-state NMR. (a) ^{15}N detected ^{1}H, ^{15}N PMLG correlation experiment including a ^{1}H T_2 filter along a third dimension τ_f. (b) H_2O–H^N spin diffusion experiment. H^N magnetization is initially suppressed using a REDOR-filter element which dephases all proton magnetization of nuclei in spatial proximitiy of a ^{15}N nucleus. Other, non–^{15}N bonded protons are not affected by the filter. A REDOR filtering time of six rotor periods is employed. A variable spin diffusion mixing time τ_{mix} allows for magnetization transfer from water protons and OH protons in the protein side chains to the amide proton which is detected in a ^{1}H, ^{15}N PMLG correlation experiment. The CP contact time is set to 160 μs to allow only for transfer between directly bonded proton and nitrogen nuclei. Filled bars refer to 90° pulses. If not otherwise indicated, open bars denote 180° pulses.

chemical shifts of the protein were taken from (van Rossum et al., 2003).

X-Ray structure determination

Diffraction images of crystals frozen in liquid nitrogen with buffer containing an additional 20% glycerol were collected at the Swiss Light Source synchrotron in Villigen, Switzerland. In the experiment, the temperature was adjusted to 100 K. For data processing, the XDS program package (Kabsch, 1993) was used. Statistics are summarized in Table 1. The structure was determined by molecular replacement using the SH3 structure deposited in the PDB (code: 1SHG) (Musacchio et al., 1992) as a model. The *R*-factors (RF) and the correlation coefficients (CC) for the first and second solution, which were found by molecular replacement using the program AMoRe (Navaza, 1994), are RF = 52.6%, CC = 0.116−RF 53.7%, CC = 0.065 after application of the rotation function, RF = 42.6%, CC = 0.474−RF = 50.7%, CC = 0.17 after application of the translation function and RF = 34.1%, CC = 0.643−RF = 48.0%, CC = 0.251 after rigid body refinement. Refinement was performed using the REFMAC5 program (Murshudov et al., 1997). Residues 5–61 could be clearly built into the electron density. For residue N47, the atoms Cγ, Oδ1 and Oδ2 of the side chain are missing due to a lack of density. Residue N47 is located in the loop region with the highest thermal displacement factors of the whole structure of approximately 29.0 $Å^2$. This is clearly above the mean value of 14.2 $Å^2$. The poor quality of the density in this region is also reflected in the torsion angles of N47 lying in the disallowed region of the Ramachandran diagram. After refinement, the *R*-factors R_{cryst} and R_{free} of the structure are 17.5% and 18.9%, respectively. The atomic displacement factors (*B*-factors) discussed below in this study indicate whether atoms deviate in position in different molecules (ensemble average) and/or whether they are flexible within one molecule (time average). Physically, the atomic displacement factor (Debye–Waller factor) is related to the mean displacement of a vibrating atom by the equation $B = 8\pi^2\langle\Delta r\rangle$. Thus, a *B*-factor of 80 $Å^2$ for an atom reflects a deviation of approximately 1 Å from the refined position.

Figures have been prepared using the program MOLMOL (Koradi et al., 1996). The structure was deposited in the PDB (entry 1U06). The data collection and refinement statistics of the X-ray structure are summarized in Table 1. H^N atoms are added to the structure using standard geometries. Characteristic distances between H^N protons and O (H_2O)/exchangeable sites in amino acid side chains were extracted from this X-ray structure and are represented in Table 2. Water molecules are numbered according to ascending *B*-factor. The lowest *B*-factor is found for W1 (16.1 $Å^2$), the highest *B*-factor is obtained for W53 (47.8 $Å^2$). Only water molecules assuming an occupancy of 100% were modelled. An interpretation of water molecules with occupancies of less than 100% – which would be indicative for actual water dynamics in the crystalline state – is not possible at the current resolution of the X-ray structure. However, the B-factor of water molecules modelled at 100% occupancy might be indicative for the exchange characteristics of water protons. In general, we expect faster proton exchange for water molecules with higher *B*-factors.

Table 1. Statistics of the X-ray structure determination of the α-spectrin SH3 domain

Data collection	
Space group	$P2_12_12_1$
Cell dimensions	a = 33.6Å, b = 42.3Å, c = 49.6 Å
Resolution*	1.49 Å (1.49 Å–1.70 Å)
Completeness	93.9%
Average $I/\sigma(I)$*	23.3 (8.9%)
R^*_{sym}	3.8% (14.8%)
Refinement	
R_{cryst}	17.5%
R_{free}	18.9%
Number of residues	55 (7–61)
Number of H_2O	53
Average atomic displacement factor (*B*-factor)	14.2 $Å^2$
rmsd bond lengths	0.010 Å
rmsd *B*-factor	0.78 $Å^2$

*Number in parentheses for highest resolution bin.

Results

We have observed previously that in the absence of homonuclear ^1H, ^1H dipolar decoupling, certain $^1H^N$ resonances are broadened in a ^1H, ^{15}N

Table 2. H^N isotropic chemical shift values, H^N T_2 decay rates and $H_2O \rightarrow H^N$ spin diffusion build-up rates for the SH3 domain of α-spectrin. $\bar{x}$ denotes the average value and σ the standard deviation fot the respective fitted parameter

Res	δ^{iso} ($^1H^N$) [ppm]	T_2 Decay		H_2O–H^N spin diffusion				Interacting protons
		T_2^{eff} [μs]		$r = I_\infty^{H_2O \rightarrow H^N}/I_0$		$T^{H_2O \rightarrow {}^{HN}}$ [μs]		
		$\bar{x}$	σ	$\bar{x}$	σ	$\bar{x}$	σ	
L8	8.0	912	102					
V9	8.8	923	51	0.327		15300		HN31/2.96;
L10	9.1							HN59/2.62;
A11	9.2							HN28/3.84 + HN29/3.73
L12	9.1							HN13/2.39
Y13	7.0	1287	316	0.217		23000		HN12/2.39
D14	8.4	1776	85	0.217		23000		O10/2.01 + HN27/3.27,
Y15	8.5	999	150	0.250		20000		O30/3.31 + HN25/2.90 + 2HZ18/3.29
Q16	7.6	1712	297	0.61	0.3	4643	3564	O26/3.95
E17	7.7			0.43	0.02	764	108	1HG24/2.55
K18	8.6	689	115					HN19/2.05
S19	7.1	473	34	0.42	0.05	1428	379	HN18/2.05 + HN22/3.53 + O25/4.74
R21	8.1							HN22/2.52 + HG19/3.40
E22	7.6	500	41	0.43	0.02	764	108	O25/3.79 + HN21/2.52 + 19/3.53
V23	7.5	1408	198					HN52/3.34
T24	6.5	502	36	0.42	0.06	1421	430	O20/3.07 + 12HH49/2.21 + 11HH49/2.81 + 1HG24/3.68
M25	9.3	1187	445	0.244		20520		HN15/2.90
K26	9.0	911	172	0.27	0.04	1352	505	O16/3.27 + O49/3.27
K27	9.2	1200	176	0.115		43336		O34/3.50 + O31/3.96 + HN14/3.23
G28	8.8	665	66	0.117		42581		O8/3.25 + HN29/2.64 + HN11/3.84
D29	8.4	584	78					O4/3.35 + HN28/2.64 + HN11/3.73
I30	8.7	593	86					*O6/4.32
L31	9.5							HN9/2.96
T32	8.2	360	39	0.48	0.03	954	153	HN45/3.14 + 1HG32/3.58 + O5/4.04 + *O6/4.44
L33	8.9	1121	69					HN7/3.37
L34	8.9	512	87	0.40	0.03	730	154	HN35/2.23
N35	7.4	533	78	0.45	0.04	2946	509	HN34/2.23 + HN43/3.12 + HN36/3.93 + *O44/4.92 + *O24/4.87

Table 2. Continued

Res	δ^{iso} ($^1H^N$) [ppm]	T_2 Decay		H_2O–H^N spin diffusion				Interacting protons
		T_2^{eff} [μs]		$r = I^{H_2O \rightarrow H^N_\infty}/I_0$		$T^{H_2O \rightarrow HN}$ [μs]		
		$\bar{x}$	σ	$\bar{x}$	σ	$\bar{x}$	σ	
S36	9.2	449	39	0.63	0.09	1768	524	O3/1.91 + O24/2.91 + HN37/2.59 + HN35/3.93 + HG36/3.46
T37	8.1	**171**	**19**	0.43	0.04	1184	282	O1/3.00 + O3/3.60 + HN36/2.59 + HN38/2.65 + 1HG37/3.46
N38	9.1	456	54	0.44	0.03	**403**	**100**	O1/1.98 + HN37/2.65
K39	8.6	423	35	0.7	0.2	5468	2291	O7/2.00 + HN40/2.45
D40	8.0	259	34	0.38	0.05	2390	652	O7/3.86 + HN41/2.26 + HN39/2.45
W41	8.4	316	28	0.44	0.11	2452	1268	HN40/2.26 + *O1/4.84
W42	9.0							HN53/3.14 + HN55/3.38
K43	8.9	541	115	0.51	0.06	1909	457	O1/3.54 + HN35/3.12
V44	9.3	1121	125	0.206		24200		HN51/2.71
E45	8.1	409	87					HN32/3.14
V46	8.9	1062	109	0.40	0.03	954	153	HN49/3.38 + HN47/3.79
R49	8.4	585	37	0.313		16000		O53/3.83 + O21/3.95 + HN48/2.52 + HN46/3.38
Q50	8.4	2281	384	0.192		26000		O23/1.97
G51	8.7	1027	87	0.219		22900		HN44/2.71
F52	9.0	1268	181	0.240		20800		O9/3.87 + HN23/3.34
V53	8.8	1129	150	0.33	0.11	3439	1975	HN42/3.14
A55	7.4	665	69	0.246		20300		O2/3.01 + HN56/2.81 + HN42/3.38
A56	7.9	500	44	0.24	0.03	567	235	O2/2.02 + O33/3.52 + HN57/2.72 + HN55/2.81
Y57	7.3	372	71					HN58/2.48 + HN56/2.72
V58	7.3	571	109	0.046		108000		HN57/2.48
K59	8.6	245	56	0.39	0.02	499	82	*O8/5.3 + *O31/5.48 + *O13/5.63 + HN10/2.62
K60	9.2	1493	257	0.169		**29500**		O11/1.96 + O51/3.98
L61	8.1	423	49	0.032		158000		HN62/2.36
D62	7.8	**2588**	**342**	0.189		26469		O/1.9 + HN61/2.36 (PDB1QKX)

Residues for which build- up rates were calculated using a linear approximation: V9, Y13, D14, Y15, M25, K27, G28, V44, R49, Q50, G51, F52, A55, V58, K60, L61, D62* water molecules adopting a distance of >4.0 Å to the respective amide proton, are not considered in the evaluation in Figure 4 and 5.

correlation experiment (Chevelkov et al., 2003). In the following, we describe two experiments that were carried out in order to characterize the origin of this effect. Both experiments are based on a ^{15}N detected PMLG ^{1}H, ^{15}N correlation experiment. ^{15}N instead of ^{1}H detection was employed in order to unambigously address the influence of water on the proton spectra.

In the first experiment, a ^{1}H T_2 filter precedes the PMLG ^{1}H evolution period (Figure 1a). Experiments were recorded using dephasing times τ_f of 0.0, 0.2, 0.4, 0.6, 0.8 and 1.2 ms. As a function of the filtering time τ_f, we observe a differential decay of the ^{1}H, ^{15}N correlation peaks (Figure 2a). Circles in the figure indicate rapidly dephasing resonances after application of a T_2 filtering time of 0.6, 0.8 and 1.2 ms, respectively. The intensity of several cross peaks as a function of the dephasing time is presented in Figure 2b. The decaying intensities were fitted assuming a mono-exponential decay according to the equation

$$I^{T2-f}(\tau_f) = I_0^{T2-f}\exp(-\tau_f/T_2^{\text{eff}}) \quad (1)$$

Intensities were normalized to the intensity I_0 of the respective cross peak at $\tau_{f=0}$ ms filtering time. The slowest decay rate is observed for residue D62 with an effective T_2 time of 2.59 ms, whereas the fastest decay rate could reliably be assigned to residue T37, which decays with an effective T_2 time of 0.17 ms. The T_2 decay rates of the H^N protons of all amino acid residues are summarized in Table 2. Note that the decay rates differ by more than a factor of 10 from one another.

In the second experiment (Figure 1b), a REDOR type filter element is employed in order to suppress all protons which are directly bonded to ^{15}N. In a subsequent mixing period (spin diffusion), magnetization is transferred from H_2O and OH protons to H^N protons which are detected again in a ^{1}H, ^{15}N correlation experiment (Figure 3). The experiment was carefully adjusted and no correlations were observed for a mixing time of $\tau_{mix=0}$ ms. Experiments were recorded using mixing times τ_{mix} of 0.0, 0.2, 0.5, 1.0, 1.5 and 5.0 ms. Build-up curves for several correlations are shown as a function of mixing time in Figure 3b. The characteristic time for H^N magnetization build-up in this experiment is represented for all amino acid residues in Table 2. The build-up rates $T^{H_2O\rightarrow H^N}$ given in Table 2 are obtained after fitting the experimental intensities $I^{H_2O\rightarrow H^N}(\tau_{mix})$ to the empirical equation

$$\frac{I^{H_2O\rightarrow H^N}(\tau_{mix})}{I_0} = r\left[1-\exp(-\tau_{mix}/T^{H_2O\rightarrow H^N})\right] \quad (2)$$

Intensities are normalized to the intensity I_0 of the respective cross peak in a regular ^{15}N detected PMLG ^{1}H, ^{15}N correlation experiment. r corresponds to the ratio of the

$$r = I_\infty^{H_2O\rightarrow H^N}/I_0 \quad (3)$$

cross peak volume $I_\infty^{H_2O\rightarrow H^N}$ obtained in the $H_2O \rightarrow H^N$ spin diffusion experiment at infinite mixing time with respect to I_0. $I_\infty^{H_2O\rightarrow H^N}$ is included as a variable parameter in the fit, since the efficiency of the spin diffusion transfer might depend on the number of protons in the vicinity of the respective H^N. The fastest build-up is observed for residue N38 with an apparent build-up time constant $T^{H_2O\rightarrow H^N}$ of 0.4 ms. For this residue, a maximum intensity of $I_\infty^{H_2O\rightarrow H^N}$ of 0.44 I_0 is obtained. The slowest build-up was determined for K60 where a value of $T^{H_2O\rightarrow H^N}$ of 29.0 ms is obtained. For approximately half of the residues, cross peaks in the $H_2O \rightarrow H^N$ spin diffusion experiment are only obtained for mixing times $\tau_{mix} \geq 5.0$ ms (i.e. V9, Y13, D14, Y15, V44, R49, Q50, G51, F52, A55, K60 and D62 etc.). For this class of residues, a linear fit – based only on the intensites at mixing times τ_{mix} = 0 and 5 ms – was employed in order to extract the respective build-up time constant $T^{H_2O\rightarrow H^N}$. For two residues, V58 and L61, a much larger value for $T^{H_2O\rightarrow H^N}$ (greater than 100 ms) is extracted from the data. This is due to the fact that the cross peak intensity in the $H_2O \rightarrow H^N$ spin diffusion experiment at τ_{mix} = 5.0 ms is very low. Longer values for τ_{mix} would have to be acquired in order to retrieve an accurate build-up time constant. Therefore, these two residues are omitted in the discussion.

In an experiment in which the spin diffusion mixing step is preceded by a t_1 evolution period and a REDOR filter, no correlations between a water molecule and an amide proton with a ^{1}H chemical shift distinct from bulk water of around 4.7 ppm could be detected (data not shown). This is due to the fact that even though oxygen atoms of water molecules are well ordered in the X-ray

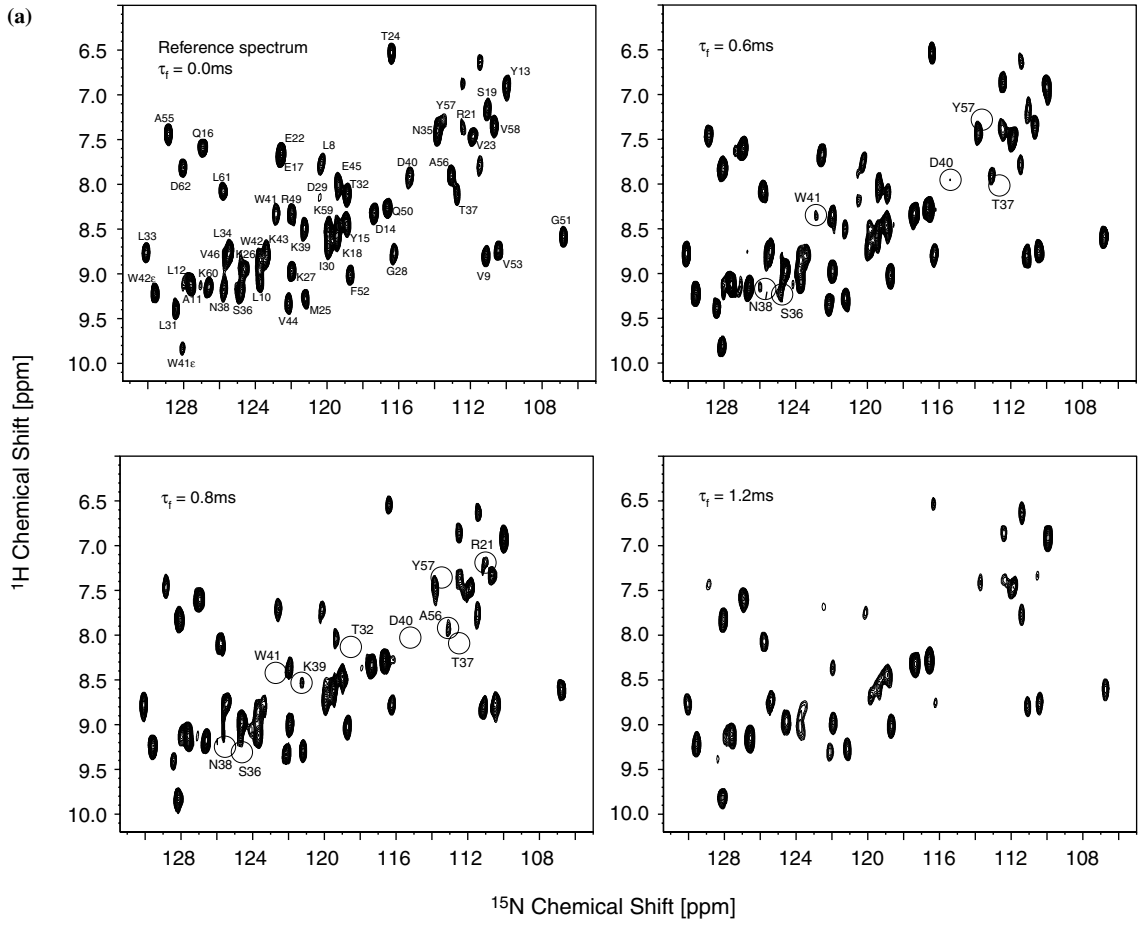

Figure 2. (a) 2D T_2 filtered ^{1}H, ^{15}N correlation spectra obtained with the pulse sequence presented in Figure 1a at various filtering times τ_f. (b) T_2 decay rates for selected residues as a function of the T_2 filtering time τ_f.

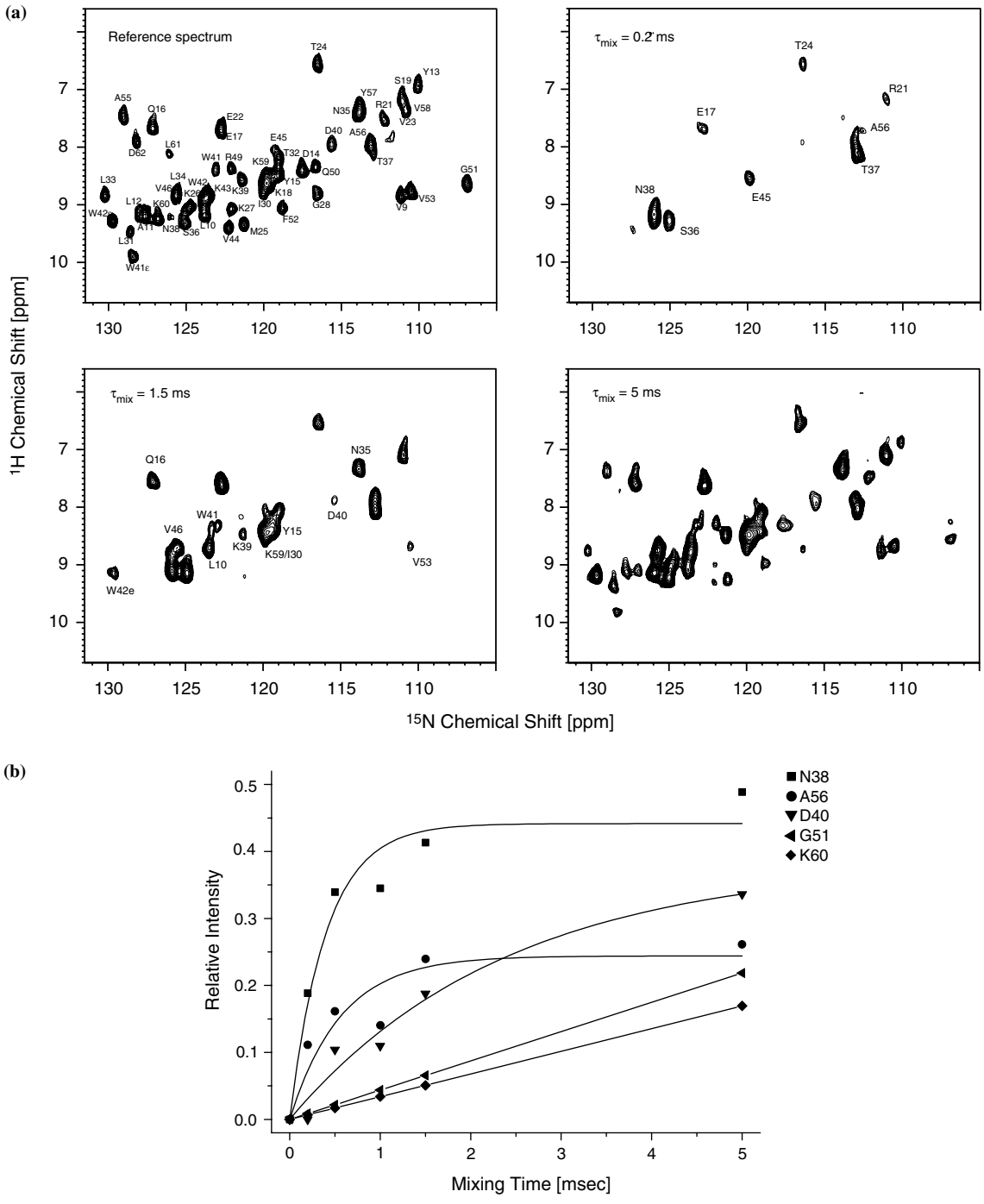

Figure 3. (a) 2D H_2O–H^N spin diffusion ^1H, ^{15}N correlation spectra obtained with the pulse sequence presented in Figure 1b at various ^1H, ^1H spin diffusion mixing times τ_{mix}. (b) Magnetization build-up curves as a function of the ^1H, ^1H spin diffusion mixing times τ_{mix} for selected residues obtained from the pulse sequence shown in Figure 1b.

structure, their protons can easily exchange with protons of water molecules from the bulk solvent background.

In order to validate the NMR data, the NMR structural parameters were interpreted in view of a high resolution X-ray structure of the wild-type

SH3 domain of chicken α-spectrin. In the original X-ray structure deposited in the PDB data base (PDB entry 1SHG, 1.80 Å resolution) (Musacchio et al., 1992) no water molecules were included. The only structure containing water molecules was determined for the mutant N47A (PDB entry 1QKX, 1.80 Å resolution) (Vega et al., 2000). Therefore, we determined the X-ray structure of the wild-type protein at a resolution of 1.49 Å (PDB entry: 1U06). Representative regions of the structure including water molecules and electron densities are represented in Figure 6.

Discussion

Inspection of Table 2 indicates that there is no simple correlation between the data of the T_2-filter and the H_2O–H^N spin diffusion experiment. The H_2O–H^N spin diffusion experiment selects protons which are not directly attached to ^{15}N. Magnetization is then transferred to the amide proton using spin diffusion mixing. We were expecting therefore that a fast build-up rate in the H_2O–H^N spin diffusion experiment should also result in a rapid T_2 decay of the respective H^N resonance. This is, however, not the case. Possible interactions for a given amide H^N are the contacts H^N–H^N, H^N–OH (side chain) and H^N–H_2O. In cases, where the respective water molecule is embedded in a network of other water molecules, the experimental H_2O–H^N build-up rate might be reduced due to dipolar truncation effects. On the other hand, the T_2-filter experiment should be especially sensitive if more than one H^N proton is in close proximity to the detected amide proton. Taken together, the two experiments yield complementary, qualitative information about the respective spin system and its dynamics.

In order to better estimate the experimental data and the correlation to the X-ray structure, we represent the relative decay or build-up rates of the two experiments as a function of the inverse third power of the ^1H, ^1H distances involved for the respective amide proton (Figure 4). The T_2 decay of the i-th proton is described semi-analytically using the equation

$$(1/T_2)^{(i)} = A + B\sum_j 1/r_{ij}^3 \qquad (4)$$

where the sum is taken over all neighboring protons j. Figure 4a represents only those amide protons for which no water molecule is found within 4 Å in the X-ray structure. Residues which have no, one and more than one dipolar interaction to another H^N proton in the protein structure are coloured white, black and green, respectively. There is apparently no correlation between the $1/T_2$ decay rate and the number of interacting protons. In order to fit the NMR experimental data, we assumed a linear relation between the $1/T_2$ decay rate and the dipolar interactions calculated from the H^N–H distances (with H being H^N, OH) as extracted from the the X-ray structure. I30, T32, W41, E45 and K59 are excluded from the fit, since they deviate significantly from the correlation. Additional residues which are in close proximity to water molecules are taken into account in Figure 4b. Red and blue symbols indicate the theoretical dipolar coupling values assuming that one and two water protons contribute to the interaction, respectively. The distance between the amide proton and the water proton is calculated according to

$$r_{ij} = \sqrt{d_{\mathrm{H^N,O}}^2 + d_{\mathrm{O,H}}^2 + 2d_{\mathrm{H^N,O}}d_{\mathrm{O,H}}\cos\phi} \qquad (5)$$

where $d_{HN,O}$ denotes the distance between H^N and water oxygen, $d_{O,H} = 0.958$ Å (Voet and Voet, 1995) the bond length in the water molecule, and ϕ the angle between the H^N—O and the O—H vector. In order to calculate the ^1H, ^1H distances, we assumed that the water oxygen is hydrogen bonded to the amide proton. In addition, we have used a value of $\phi = 52.25°$ (Voet and Voet, 1995), assuming symmetrically bound water molecules. The experimental T_2 decay data, taking water molecules into account, fit the same empirical relation, with the exception of residues D14, Q50, K60, A56 and S36. For these H^N protons, a long effective T_2 is observed, even though water molecules are found in close proximity. So far, the isotropic and anisotropic H^N chemical shifts, as well as their orientations are not taken into account in the analysis of the T_2 decay rates. The observed deviations might be due to a $n = 0$ rotational resonance effect (Levitt et al., 1990). Therefore, the $1/T_2$ decay rate was analyzed as a function of the H^N, H^N chemical shift difference ($\Delta\delta$) (Figure 4c). The projection angle between the

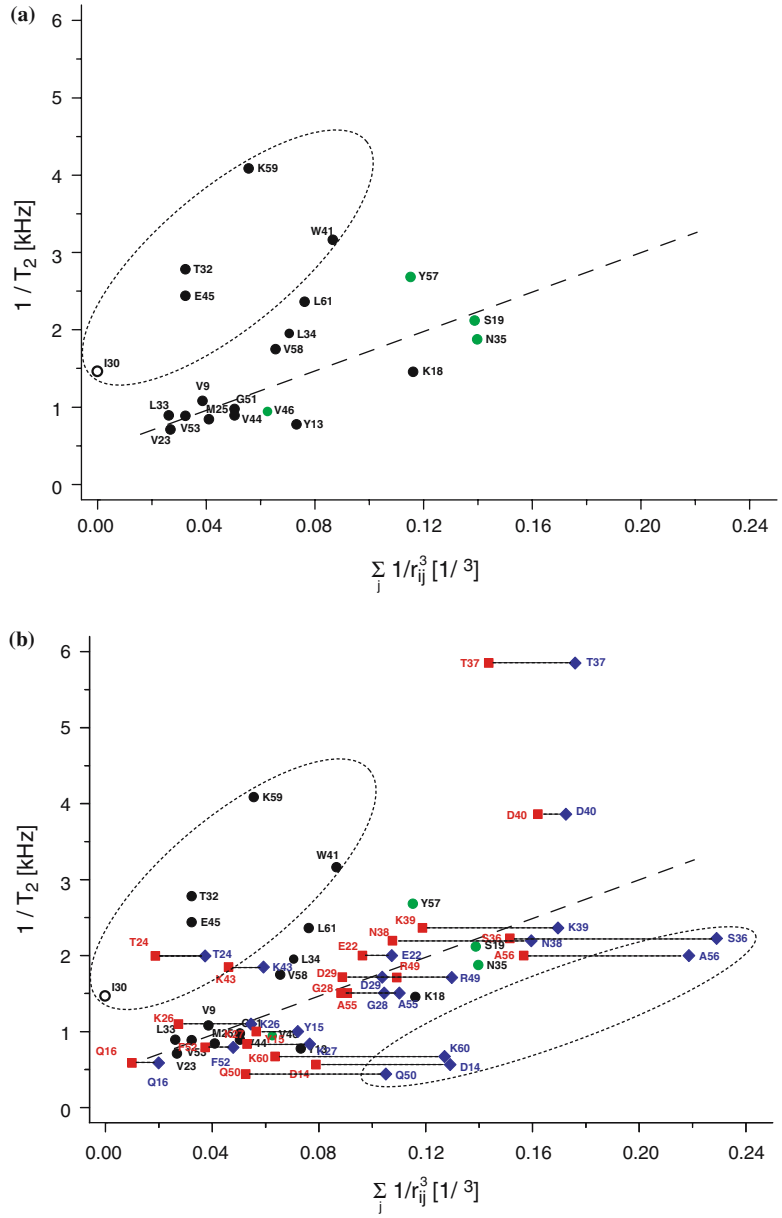

Figure 4. Effective $1/T_2$ dephasing rate as a function of the dipolar interactions as expected from the X-ray structure. (a) Only residues are represented for which no water molecule is found within 4.0 Å. Residues which have no, one and more than one dipolar interaction to another H^N proton in the protein structure are coloured white, black and green, respectively. (b) All residues are represented. Red and blue symbols indicate the theoretical dipolar coupling values assuming that one and two water protons contribute to the interaction, respectively. (c) $1/T_2$ relaxation rate as a function of the isotropic chemical shift difference between two H^N protons. Only the strongest interaction is taken into account in cases where a H^N proton is in close proximity to two H^N protons. A grey box indicates isotropic chemical shift differences of less than 200 Hz ($\equiv$ 0.3 ppm), indicating the experimental H^N line width. Residues for which the H^N atom is in contact with another H^N atom within $<$2.5 Å, 2.5–3.0 Å and 3.0–3.5 Å are coloured in red, green and blue, respectively.

two respective H^N–N vectors which are in spatial proximity and which might be an approximation for the differential ^1H chemical shift anisotropy (CSA) is represented in the figure as well. Residues for which the H^N atom is in contact with another H^N atom within 2.0–2.5 Å, 2.5–3.0 Å and 3.0–3.5 Å are coloured in red, green and blue, respectively. In cases where a H^N proton is in the

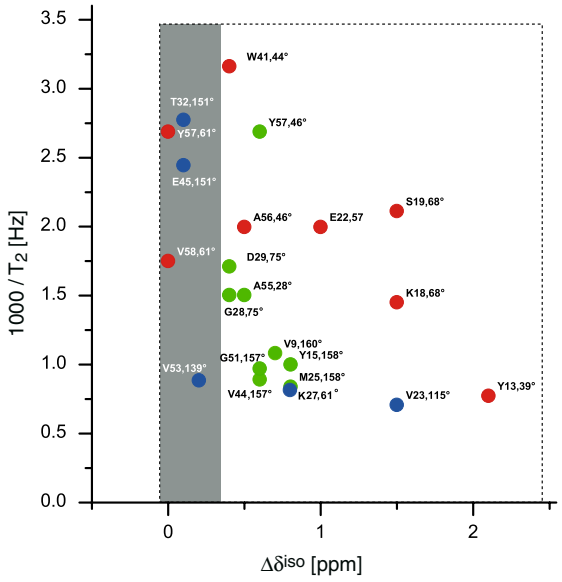

Figure 4. Continued

vicinity of two amide protons, only the strongest interaction is taken into account (Y57 is represented twice, since its amide proton is found to be within 2.5 Å distance to A56H^N and V58H^N). For small chemical shift differences, a slight increase in the rate is observed as expected (e.g. T32, Y57, E45). The range of the $n=0$ rotational resonance effect is defined by the line width of the respective H^N resonance which is on the order of 200 Hz (≡ 0.3 ppm), indicated by a box coloured in grey. On the other hand, a large dispersion of $1/T_2$ decay rates is observed for H^N protons for which only a small isotropic chemical shift difference between the dipolar coupled nuclei is observed (residues coloured in green, corresponding to a H^N, H^N distance of 3.0–3.5 Å). We therefore conclude that mechanisms other than the $n=0$ rotational resonance must contribute to the $1/T_2$ decay rate.

In Figure 5a, the NMR experimental H$_2$O–H^N build-up rate is correlated with the dipolar couplings calculated from the H$_2$O–H^N distances extracted from the X-ray structure according to Equation 5a. For completeness, Figure 5b represents the maximum intensity $I^{\infty}_{\mathrm{REDOR-f}}/I_0$ that can be achieved for each ^{1}H, ^{15}N correlation peak as a function of the $1/T^{(\mathrm{H_2O}\rightarrow\mathrm{H^N})}$ build-up rate. For very long mixing times, this ratio should provide information on the number of water protons in the vicinity of the respective H^N proton (for one proton, a value of 0.5 would be expected; for 2 protons 0.67 etc.). At first sight, the build-up rate does not seem to be related to the expected dipolar interactions. However, taking into account that water molecules can be classified according to their binding properties with respect to the protein allows an identification of three distinct types of water molecules (in addition to bulk water):

(I) Water molecules being in contact with bulk solvent (region I). For residues D14, Q50, and K60, we observe a very small build-up rate $1/T^{(\mathrm{H_2O}\rightarrow\mathrm{H^N})}$ (Figure 5a). At the same time, $1/T_2$ adopts a smaller value than expected from the distances extracted from the X-ray structure (Figure 4b). The crystal structure displays a very dense network of water molecules around these residues. This network of water molecules is located on the surface of the protein and is in contact with bulk solvent (Figure 6). We explain the observed deviations by postulating that water protons near residues found in region I are in very fast exchange with bulk solvent water molecules. This would result in a reduction of dipolar interactions. Therefore, these water molecules do not contribute significantly to a magnetization build-up in the H$_2$O–H^N spin diffusion experiment nor to the H^N T_2 decay, and are not detectable by MAS solid-state NMR.

(II) Tightly bonded water within the core of the protein (region II). Water molecules associated with region II (T37, N38, A56 etc.), follow an empirical $1/r^3$ relation between the $1/T^{(\mathrm{H_2O}\rightarrow\mathrm{H^N})}$ build-up rate and the dipolar interaction expected from distances extracted from the X-ray structure. These water molecules behave solid-like. Most of them have contacts to a symmetry-related molecule in the crystal. They can therefore be considered as being located in a pseudo-core of the protein. Figure 6b displays the electron densities around N38. The amide proton of N38 is hydrogen bonded to W1, the water molecule with the lowest *B*-factor in the X-ray structure. In addition, N38 is close to many other water molecules (W3 and W9 of a symmetry-related molecule). From the structure, we expect that protons from W1 are protected from exchange with protons from bulk solvent, since N38 is involved in crystal contacts to a symmetry related SH3 molecule. Similar arguments are applicable to T37 and A56.

(III) Dynamic water molecules (region III). For residues which are located in region III (E22, V46 etc.), we find a very rapid magnetization build-up in

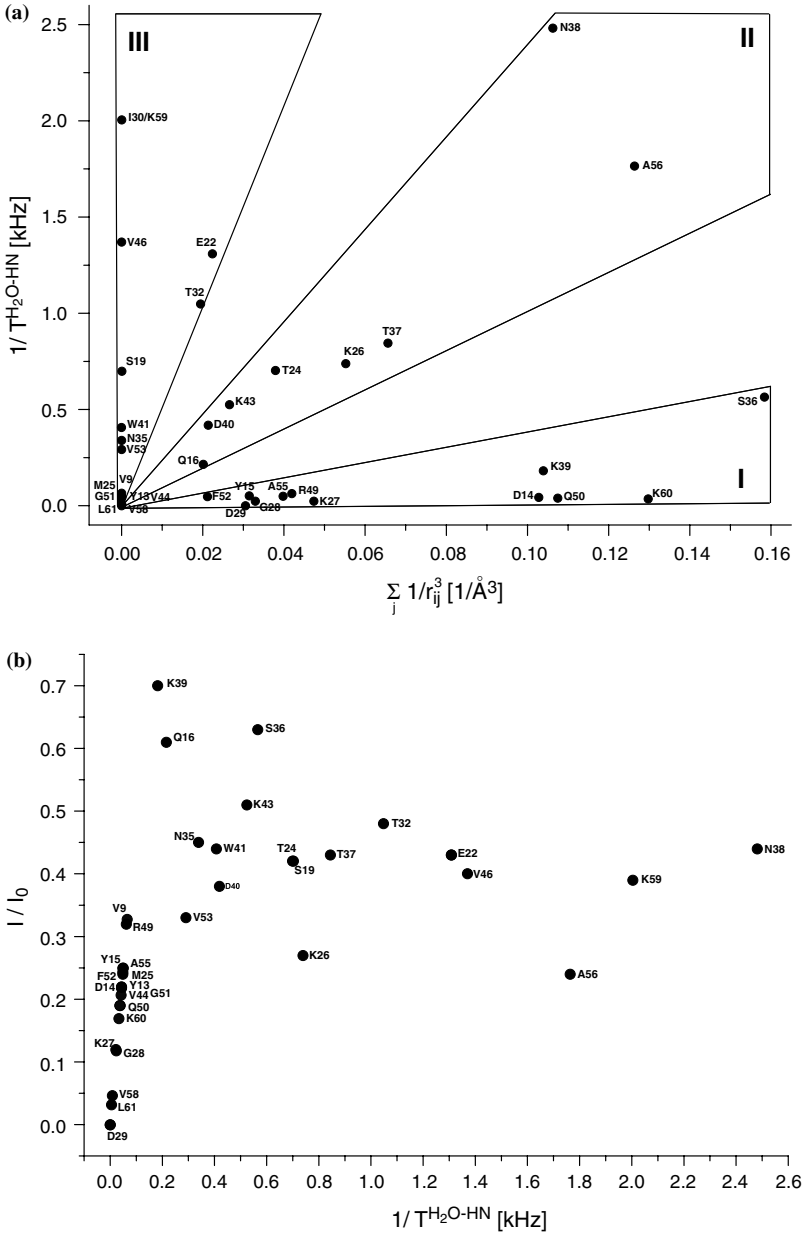

Figure 5. (a) H_2O–H^N spin diffusion build-up rates as a function of the expected dipolar interactions. Amide protons which are in contact with bulk water, ordered water and flexible regions of the protein are labeled with I, II and III, respectively. (b) Ratio r between cross peak volumes $I^{\infty}_{\mathrm{REDOR-f}}$ in the H_2O–H^N spin diffusion experiment (intensity at equilibration) and I_0 in the ^1H, ^{15}N PMLG correlation reference experiment, as a function of the experimental H^N $1/T_2$ decay rate.

the $H_2O \rightarrow H^N$ spin diffusion experiment, although no interaction partner (H^N, OH or H_2O) is found in the respective region of the X-ray structure. We postulate that this fast build-up arises from dynamic water molecules which are not detectable in the X-ray structure. V46 is located in a loop region which connects β-strands 3 and 4 (Figure 6c). For this loop, a higher mean B-factor of 25.5 $Å^2$ is found (residues 46–49) compared to the average B-factor of the structure of 14.2 $Å^2$. Interestingly, no ^1H, ^{15}N correlations for N47 (mean B-factor = 29.0 $Å^2$) and D48 (mean B-factor = 26.0 $Å^2$) could be assigned in the MAS solid-state NMR spectra. Figure 6a displays the SH3 structure, colour coded

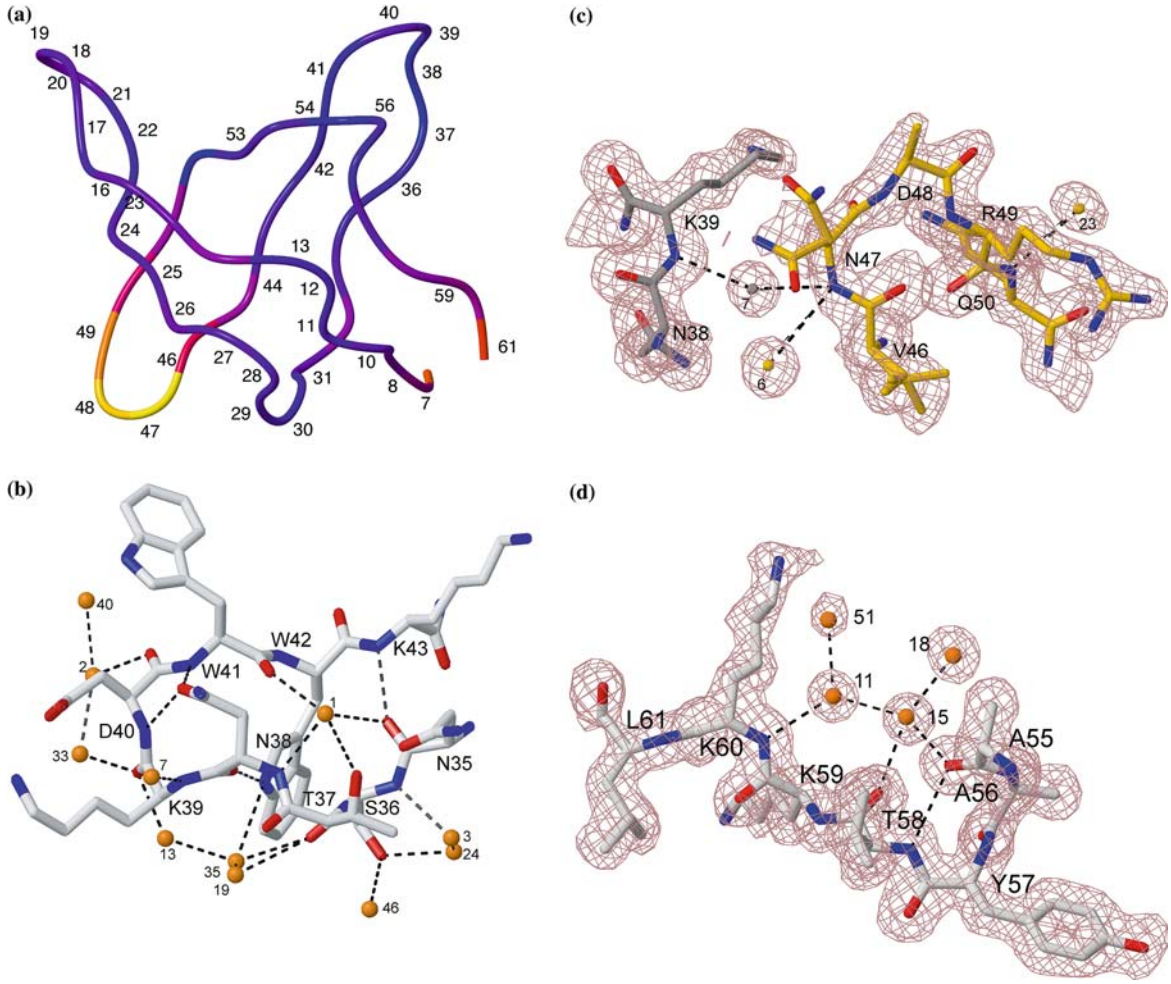

Figure 6. C^{α} backbone representations of the crystal structure of the chicken α-spectrin SH3 domain. (a) Colour coding is according the X-ray *B*-factor. *B*-factors of around 10, 20 and 30 $Å^2$ are represented in blue, red and yellow, respectively. (b)–(d) Refined structure and experimental electron densities ($2F_O - F_C$, brown) contoured at 1.0 σ for selected residues (V46 and K60). For clarity, residue N38 is represented without density. In case of V46/N47, the molecule in the unit cell is coloured in yellow, whereas the symmetry related molecule is coloured in grey.

according to the *B*-factors from the X-ray data refinement. In the current electron density refinement, only water molecules are taken into account that have an occupancy of 100%. Water molecules which undergo chemical exchange between two or more sites have an occupancy of less than 100% and cannot be detected in the X-ray structure at the current resolution. In addition to dipole–dipole interactions, which are expected for protons in the solid-state yielding a $1/r^3$ dependence, fluctuations of dipolar interactions inducing relaxation might have to be taken into account for these mobile water molecules. Magnetic relaxation dispersion allows for the determination of the correlation time of water molecules in the core of a protein (Halle and Denisov, 2001). The correlation time could be estimated to be on the order of $\tau_c \approx 1\mu s$. Motion of water molecules on this time scale should induce relaxation in neighbouring H^N resonances due to fluctuations of dipole dipole interactions. Such motion would be in agreement with the observation of disordered regions in the protein crystal in which the electron densities are not very well defined indicating small conformational heterogeneities. We cannot totally rule out the possibility that differences observed between the solid-state NMR data and the X-ray crystal structure are due to the different temperatures which are used in the X-ray

(100 K) and NMR studies (280 K), respectively. In order to unambiguously address this question, a room temperature X-ray structure would be required. We expect, however, that for a X-ray structure determined at 280 K, the discrepancies in region III between the NMR and the X-ray data would be even more striking, since the number of well defined water molecules would be lower due to increased thermal motion.

For four residues (E17, R21, T32 and S36), side chain exchangeable protons are close to individual amide protons in the backbone: E17 ($E17H^N$–T24OH, 2.6 Å), R21 ($R21H^N$–S19OH, 2.7 Å), T32 ($T32H^N$–T32OH, 3.4 Å) and S36 ($S36H^N$–S36OH, 2.3 Å). So far, we were not able to detect the corresponding side chain protons in a direct or indirect fashion. These interactions are not taken into account in Figure 4a and 5a. We expect, however, that contributions due to side chain exchangeable protons are small due to fast dynamics. Suppression of exchange relayed transfers ($H_2O \rightarrow OH \rightarrow H^N$) is theoretically possible, but requires the application of periodic band-selective decoupling pulses covering the entire ^1H chemical shift range from 12 to 6 ppm (Cai et al., 2003). In this study, application of these pulses is not possible, since this pulse would as well affect the water–H^N correlations. However, such applications to deuterated protein samples with selective methyl group protonation (Rosen et al., 1996) are possible to suppress these unwanted correlations.

Previously, ^1H, ^{13}C exchange correlations were observed between side chains containing labile protons and water (Lesage and Böckmann, 2003). We can exclude that chemical exchange during cross-polarization contributes significantly to the H_2O–H^N build-up rate. Exchange rates between amide protons and the solvent are typically on the order of <10 Hz (Gemmecker et al., 1993). In addition, we did not observe cross peaks between water and amide nitrogens using a CP contact time between 160 μs and 2 ms in a ^1H, ^{15}N PMLG correlation experiment. We therefore conclude that the effects that we observe are due to ^1H, ^1H homonuclear couplings.

Conclusion

We have shown that MAS solid-state NMR can provide information about water molecules in a protein structure undergoing dynamics on different timescales. Interpretation of the NMR data in view of the X-ray structure of the SH3 domain resulted in a classification of three types of water molecules which are assigned to (1) water involved in hydrogen networks close to bulk water on the surface of the protein, to (2) water buried in the interior of the protein and to (3) mobile water molecules located in flexible regions of the molecule. Analysis of the H_2O–H^N spin diffusion build-up experiment allows the assignment of dynamic water molecules. Water molecules which are located on the surface of the protein and which exchange rapidly with the bulk solvent are not detected. Analysis of the H^N T_2 decay rates show that this experiment is sensitive both to H^N, H^N and H^N, H_2O interactions. In cases where the X-ray structure is not known, short H^N, H^N distances are readily identified as described earlier (Reif et al., 2003). This should allow a differentiation between H^N, H^N and H^N, H_2O contacts, and therefore an identification of water molecules. We expect that these experiments will find use in order to better understand the role of water in stabilizing protein structures.

Acknowledgements

This work was supported by DFG grant Re1435 and by the Fonds der Chemischen Industrie. We thank Dr Clemens Schulze-Briese and Dr Mariana Oetiker, Swiss Light Source, Villigen, Switzerland, for assistance in collecting the X-ray data.

References

Bak, M., Rasmussen, J.T., and Nielsen, N.C. (2000) *J. Magn. Reson.*, **147**, 296–330.

Bennett, A.E., Rienstra, C.M., Auger, M., Lakshmi, K.V., and Griffin, R.G. (1995) *J. Chem. Phys.*, **103**, 6951–6958.

Cai, S., Stevens, S.Y., Budor, A.P., and Zuiderweg, E.R.P. (2003) *Biochemistry*, **42**, 11100–11108.

Castellani, F., Rossum, B.-J.van, Diehl, A., Schubert, M., Rehbein, K., and Oschkinat, H. (2002) *Nature*, **420**, 98–102.

Chevelkov, V., Rossum, B.J.V., Castellani, F., Rehbein, K., Diehl, A., Hohwy, M., Steuernagel, S., Engelke, F., Oschkinat, H., and Reif, B. (2003) *J. Am. Chem. Soc.*, **125**, 7788–7789.

Clore, G.M., Bax, A., Wingfield, P.T., and Gronenborn, A.M. (1990) *Biochemistry*, **29**, 5671–5676.

Denisov, V.P., Peters, J., Hörlein, H.D., and Halle, B. (1996) *Nat. Struct. Biol.*, **3**, 505–510.

Gemmecker, G., Jahnke, W., and Kessler, H. (1993) *J. Am. Chem. Soc.*, **115**, 11620–11621.
Gottschalk, M., Dencher, N.A., and Halle, B. (2001) *J. Mol. Biol.*, **311**, 605–621.
Halle, B., and Denisov, V.P. (2001) *Meth. Enzymol.*, **338**, 178–201.
Harbison, G.S., Roberts, J.E., Herzfeld, J., and Griffin, R.G. (1988) *J. Am. Chem. Soc.*, **110**, 7221–7223.
Kabsch, W.J. (1993) *J. Appl. Cryst.*, **26**, 795–800.
Koradi, R., Billeter, M., and Wüthrich, K. (1996) *J. Mol. Graph.*, **14**, 51–55.
Lesage, A., and Böckmann, A. (2003) *J. Am. Chem. Soc.*, **125**, 13336–13337.
Lesage, A., and Emsley, L. (2001) *J. Magn. Reson.*, **148**, 449–454.
Levitt, M.H., Raleigh, D.P., Creuzet, F., and Griffin, R.G. (1990) *J. Chem. Phys.*, **92**, 6347–6364.
McDermott, A., Polenova, T., Böckmann, A., Zilm, K.W., Paulsen, E.K., Martin, R.W., and Montelione, G.T. (2000) *J. Biomol. NMR*, **16**, 209–219.
Murata, K., Mitsuoka, K., Hirai, T., Walz, T., Agre, P., Heymann, J.B., Engel, A., and Fujiyoshi, Y. (2000) *Nature*, **407**, 599–605.
Murshudov, G.N., Vagin, A.A., and Dodson, E.J. (1997) *Acta Cryst.*, **D53**, 240–255.
Musacchio, A., Noble, M.E.M., Pauptit, R., Wierenga, R.K., and Saraste, M. (1992) *Nature*, **359**, 851–855.
Navaza, J. (1994) *Acta Cryst.*, **A50**, 157–163.
Noack, F. (1986) *Prog. NMR Spect.*, **18**, 171–276.
Noack, F., Becker, S., and Struppe, J. (1997) *Annu. Rep. NMR Spectrosc.*, **33**, 1 .
Otting, G. (1997) *Prog. Nucl. Magn. Reson. Spectrosc.*, **31**, 259–285.
Otting, G., and Wüthrich, K. (1989) *J. Am. Chem. Soc.*, **111**, 1871–1875.
Pauli, J., Baldus, M., Van Rossum, B.-J., De Groot, H., and Oschkinat, H. (2001) *Chem. BioChem.*, **2**, 272–281.
Pauli, J., Van Rossum, B.-J., Förster, H., De Groot, H.J.M., and Oschkinat, H. (2000) *J. Magn. Reson.*, **143**, 411–416.
Paulson, E.K., Morcombe, C.R., Gaponenko, V., Dancheck, B., Byrd, R.A., and Zilm, K.W. (2003) *J. Am. Chem. Soc.*, **125**, 14222–14223.
Paulson, E.K., Morcombe, C.R., Gaponenko, V., Dancheck, B., Byrd, R.A., and Zilm, K.W. (2003) *J. Am. Chem. Soc.*, **125**, 15831–15836.
Reif, B., and Griffin, R.G. (2003) *J. Magn. Reson.*, **160**, 78–83.
Reif, B., Jaroniec, C.P., Rienstra, C.M., Hohwy, M., and Griffin, R.G. (2001) *J. Magn. Reson.*, **151**, 320–327.
Reif, B., Rossum, B.J.van, Castellani, F., Rehbein, K., Diehl, A., and Oschkinat, H. (2003) *J. Am. Chem. Soc.*, **125**, 1488–1489.
Rienstra, C.M., Tucker-Kellogg, L., Jaroniec, C.P., Hohwy, M., Reif, B., McMahon, M.T., Tidor, B., Lozano-Pérez, T., and Griffin, R.G. (2002) *Proc. Natl. Acad. Sci. USA*, **99**, 10260–10265.
Rosen, M.K., Gardner, K.H., Willis, R.C., Parris, W.E., Pawson, T., and Kay, L.E. (1996) *J. Mol. Biol.*, **263**, 627–636.
Saparov, S.M., and Pohl, P. (2004) *Proc. Natl. Acad. Sci. USA*, **101**, 4805–4809.
Rossum, B.-J.van, Castellani, F., Pauli, J., Rehbein, K., Hollander, J., De Groot, H.J.M., and Oschkinat, H. (2003) *J. Biomol. NMR*, **25**, 217–223.
Vega, M.C., Martinez, J.C., and Serrano, L. (2000) *Prot. Sci.*, **9**, 2322–2328.
Vinogradov, E., Madhu, P.K., and Vega, S. (1999) *Chem. Phys. Lett.*, **314**, 443–450.
Voet, D., and Voet, J.G. (1995) *Biochemistry, 2nd edn*, John Wiley and Sons, New York.
Zhou, Y., Morais-Cabral, J.H., Kaufman, A., and MacKinnon, R. (2001) *Nature*, **414**, 43–48.